Eur. Phys. J. C (2025) 85:382
https://doi.org/10.1140/epjc/s10052-025-14098-w

THE EUROPEAN PHYSICAL JOURNAL C

Regular Article - Theoretical Physics

Topological constraints on general relativistic galaxy modelling

Marco Galoppo[a]

School of Physical and Chemical Sciences, University of Canterbury, Private Bag 4800, Christchurch 8041, New Zealand

Received: 16 October 2024 / Accepted: 19 March 2025

Abstract We study the impact on the average rotational dynamics and gravitational lensing of topological structures within fully general relativistic galaxy models. These topological structures do not possess a Newtonian analogue and, therefore, represent a purely general relativistic feature which could a priori impact galactic observables. We characterise these structures both for rigidly rotating and differentially rotating solutions. By employing GAIA DR3 data, we find that such topological defects can impact the transition between the rising and flat regimes of the galaxy. Furthermore, we show that topological defects produce a noticeable increase in the deflection angle produced by Milky Way-like galaxies. Finally, we find that topological singularities can be avoided within the class of differentially rotating solutions.

1 Introduction

General Relativity (GR) is the currently accepted theory of gravity and a crowning achievement of theoretical physics of the 20th century. GR has passed all the experimental and observational tests the scientific community could devise [1]. Even its most outlandish predictions, such as neutron stars [2,3], black holes [4–6] and gravitational waves [7,8], have been confirmed by astrophysical observations. The picture of reality emerging from GR has deeply changed our knowledge of the local and far Universe, introducing novel elements with no direct analogues in the Newtonian theory of gravity, e.g., a curved spacetime.

It is clear that in extreme astrophysical events, new phenomena arise which do not possess any Newtonian analogue, and yet can still drive the dynamics of the systems. Indeed, this is precisely the case for the coalescence of black hole binaries via gravitational wave emissions. However, even in the case of weak-gravitational fields purely GR effects exist which do not possess a Newtonian counterpart, e.g., the gravitomagnetic effects related to mass currents and spacetime rotation [9,10].

We note that it is generally false that GR effects are always negligible w.r.t. the corresponding Newtonian ones, since the latter at times might simply not exist. Moreover, even if Newtonian analogues exist, the situation is not always straightforward. In fact, if we consider the gravitational lensing by a point-like source, we find that the bending angle calculated within the Newtonian framework differs by a factor of two from the general relativistic one [11]. Hence, in this simple case, the Newtonian and the GR effect are of the same order of magnitude. It is then natural to wonder in which novel, and perhaps unexpected, astrophysical setting GR effects could significantly differ once more from Newtonian predictions.

In particular, the role of peculiar GR effects in the dynamics of disc galaxies has become a contentious point and is currently being discussed in various papers. Conventionally, GR corrections to the Newtonian dynamic of disc galaxies are considered to be negligible. This stance directly follows from (i) the assumption that in a low-energy regime, GR reduces to its linearised version, which can be effectively superimposed with Newtonian gravity, and (ii) the important result that linearised GR does not produce significant corrections to the predicted disc galaxies rotation curves from the baryonic matter content alone [12,13].

However, some authors argue that the presence of non-negligible off-diagonal components in the global galactic metric – i.e., the presence of a strong dragging vortex surrounding disc galaxies, with no Newtonian analogue – could return important corrections on the crucial measures of disc galaxy rotation curves, even in a low-energy regime. In other words, GR would allow for disc galaxy rotation sustained for a relevant fraction by the spacetime frame-dragging, coupled to the usual centripetal attraction of the matter within the galaxy [14–30].

[a] e-mail: marco.galoppo@pg.canterbury.ac.nz (corresponding author)

Published online: 03 April 2025

Within this framework, Cooperstock and Tieu [14,15] and then Balasin and Grumiller [16] presented pressureless, rigidly rotating full GR galaxy models. However, the Cooperstock and Tieu model was proven to contain highly non-physical features, surpassed in the later Balasin and Grumiller model (BG).

Here, we stress that BG cannot be considered a valid, global disc galaxy model. To wit, by its very design, BG cannot model the galaxy bulge as close encounters of stars are frequent enough to invalidate treating matter as a pressureless fluid, i.e., dust. Moreover, the modelling of the vertical gravity in disc galaxies is, at the very least, dubious within a model devoid of internal, effective pressure. Furthermore, the rigid rotation assumption [16] directly leads to unphysical features, e.g., the null expected red-shift with respect to the asymptotic Minkowskian observers [21,27,31] as well as unreasonably large time delays in gravitational lensed images on the equatorial plane [24]. Finally, as already pointed out in [16] and studied further in [31], the BG model presents two naked singularities along the rotation axis, outside the galactic plane, i.e., two NUT rods linked by a cosmic string.

Nonetheless, as discussed in [17], and further clarified in [26], the presence of curvature singularities can be neglected whilst fitting data on the equatorial plane as "*the solution was found in the disc region in a different regime*" [26]. That is, BG must be considered exclusively as a *local* model for the thin disc alone of a disc galaxy. Then, the presence of timelike curvature singularities far away from the thin disc will not influence the fit to observational data, given the local nature of GR (see also the seminal paper by Neugebauer [32]). Indeed, starting from this premise, Crosta and coworkers [17,26] presented a fit of BG to the Milky Way (MW) rotation curve reconstructed from the GAIA satellite's kinematic DR2 and DR3 data. BG was shown to fit the data without need for dark matter (DM) and was ultimately considered equivalent to DM-driven galactic dynamics.

However, even if considered as only a local, thin disc model, BG does not clear the criticism about the null red-shift measurements by a distant observer [27,31,33]. This is due to its unphysical rigid rotation, which we believe to ultimately disqualify the model. Furthermore, even if BG were employed exclusively as a rough approximation, important topological issues have been overlooked in the previous literature, which need to be addressed to better inform the scientific debate on the validity of full GR modelling of galaxies. Indeed, in this paper we show the presence of non-isolated topological defects [34,35] – with no Newtonian analogue – within the whole class of pressureless, rigidly rotating solutions to the Einstein field equations (EFE), i.e., the van Stockum–Bonner (vSB) [36–38] class. For BG, we show that the presence of such singularities directly impacts the fitting of the GAIA DR3 data, as well as lensing calculations.

Finally, to bypass the deficiencies brought about by rigid rotation, the field is shifting its focus to the full class of stationary, axisymmetric, dust solutions of the EFE which allow for differential rotation in the modelled galaxy [19,21–23,27–29]. These models improve upon some of the problematic features of BG [31,33], e.g., the null red-shift problem. However, as these solutions do not yet include an effective internal pressure within the galaxy,[1] they cannot yet be reasonably employed in modelling the bulge regions of disc galaxies or in precise studies of their vertical gravity. Nonetheless, we stress that they could be employed to model thin, bulgeless disc galaxies. However, a first step in further developing these models to the non-zero pressure case has been taken in [30], where an internal effective pressure has been introduced at the first order. In this paper, we also investigate the wider class of differentially rotating solutions and provide the necessary conditions that such models must meet to avoid the presence of both curvature and topological singularities along the axis of rotation. Thus, we consider for the first time the presence of topological structures – absent within the Newtonian framework – also within the general differentially rotating GR galaxy models.

The rest of the paper is structured as follows. In Sect. 2 we introduce the concept of quasi-regular singularities and conical singularities; in Sect. 3 we define the general class of stationary, axisymmetric, dust solutions of EFE, with a particular focus to the vSB subclass; in Sect. 5 we prove the existence of non-isolated quasi-regular singularities in the vSB subclass; in Sect. 6 we specialise to the BG model, and derive the topological defects impact on the rotation curve fitting of GAIA DR3 data and in-plane gravitational lensing; in Sect. 7 we derive the conditions for pressureless, differentially rotating solutions to avoid such pathologies; Sect. 8 is dedicated to a brief overview of the results and future perspectives.

2 Topological singularities

A point q of a spacetime $(M, \boldsymbol{g})$ is defined as a quasi-regular singularity – a topological singularity – if it is the end point of an incomplete geodesic $\gamma(\lambda)$, where λ is a generalised affine parameter, and it is not a curvature singularity [34,35]. The curvature components $R_{\mu\nu\rho\sigma}$ measured in an orthonormal frame are bounded in q. However, these can still present discontinuities related to the presence of delta-type mass distributions, which can give rise to such singularities [34,40]. Nonetheless, quasi-regular singularities are undetectable from local considerations. The spacetime is locally

[1] Disc galaxy, although collisionless systems outside the bulge, are not pressureless [39]. For example, it is the effective internal pressure within these systems which maintains the thickness of the disc.

Minkowskian next to a topological singularity, yet their presence is imprinted on the global geometrical structure of the spacetime via geodesic focusing [34,40].

In particular, we are interested in the quasi-regular singularities named conical singularities, such as the one identified by the tip of a cone. To understand their nature, let us consider Minkowski spacetime in cylindrical coordinates

$$\mathrm{d}s^2 = -c^2\,\mathrm{d}t^2 + \mathrm{d}r^2 + r^2\,\mathrm{d}\phi^2 + \mathrm{d}z^2, \tag{1}$$

where $t, z \in (-\infty, \infty)$, $r \in [0, +\infty)$ and $\phi \in [0, 2\pi]$. To obtain a conical singularity from this spacetime, we may proceed by identifying points related by the translation [34, 40]

$$\phi = \phi + \alpha, \tag{2}$$

where $\alpha \neq 2\pi$. This results in a new spacetime with a metric locally equivalent to (1) but globally different, for which $t, z \in (-\infty, \infty)$, $r \in [0, +\infty)$ and $\phi \in [0, \alpha]$. The points on the z-axis in this new spacetime are conical singularities. To gauge their singular nature, we can compute the circumference-to-radius ratio of any circle drawn around the z-axis on a 2-surface $\{t = const, z = const\}$ in the limit $r \longrightarrow 0$. Doing so gives a ratio equal to α instead of the Euclidean 2π. These singularities result in a focusing (attractive) effect for $\alpha < 2\pi$, and a defocusing (repulsive) effect for $\alpha > 2\pi$. The presence of conical singularities in a spacetime can be directly inferred whenever the angular coordinate satisfies $\phi \in [0, 2\pi]$, and the line element can be cast in the form

$$\mathrm{d}s^2 = -c^2\,\mathrm{d}t^2 + \mathrm{d}r^2 + f^2\,r^2\,\mathrm{d}\phi^2 + dz^2. \tag{3}$$

The line element in (3) is locally equivalent to the one of (1) but with $0 < \phi < 2\pi f$, as can be seen by the change of coordinates $\phi' = f\,\phi$. Therefore, the identification of conical singularities is easily achieved, if it is possible to write the line element in a form equivalent to (3), as in the case of cosmic strings [40–42]. However, this is generally not possible and more complex procedures are required to identify conical singularities, e.g., calculating the holonomy group of the manifold for the suspected singular points [43]. In our study, we make use of a well known result for stationary, axisymmetric spacetimes [44]. These geometries present conical singularities whenever the regularity condition

$$\frac{X_{,\mu}X^{,\mu}}{4\,X} \longrightarrow 1, \tag{4}$$

is violated, where $X = \xi_\mu \xi^\mu$ with $\boldsymbol{\xi}$ as the Killing vector associated to the axial symmetry, and the limit is taken at the rotation axis. If (4) is satisfied by the spacetime then Lorentzian geometry is ensured near the rotation axis, otherwise, conical singularities are present along the axis. However, we must highlight that even if a spacetime does meet the regularity condition (4), this does not preclude further topological defects from being present outside the z axis.

3 Galaxy models

In full GR modelling of galaxies, we consider an idealised version of the physical system that is in stationary motion, with exact symmetry around its rotation axis. This neglects the morphological evolution of the galaxy, and any structure that breaks the axisymmetry (e.g., bars or spirals). Hence, spacetime possesses two Killing vectors, generating the time translation and the rotation around the axis, which allow a clear definition of the two coordinates t and ϕ. The parametrisation of the spacetime is then completed by the distance z from the galactic plane $z = 0$, and the distance r from the z axis. The metric takes the Lewis–Papapetrou–Weyl form [44]

$$\begin{aligned}\mathrm{d}s^2 &= -c^2 e^{2\Phi(r,z)/c^2}(\mathrm{d}t - A(r,z)\,\mathrm{d}\phi)^2 \\ &\quad + e^{-2\Phi(r,z)/c^2}\left[W(r,z)^2\,\mathrm{d}\phi^2 + e^{2k(r,z)/c^2}(\mathrm{d}r^2 + \mathrm{d}z^2)\right] \\ &= -c^2 e^{2\nu(r,z)/c^2}\,\mathrm{d}t^2 + g_{\phi\phi}(r,z)(\mathrm{d}\phi - \chi(r,z)\,\mathrm{d}t)^2 \\ &\quad + e^{\mu(r,z)/c^2}(\mathrm{d}r^2 + \mathrm{d}z^2),\end{aligned} \tag{5}$$

where $\Phi(r, z)$ is the pseudo-Newtonian potential, $A(r, z)$ is related to frame-dragging, $k(r, z)$ is a conformal factor on the two-dimensional space of orbits of the isometry group generated by the Killing vectors and $W(r, z)$ further specialises the angular geometry. In the second line of (5), we have defined $g_{\phi\phi} = W^2 e^{-2\Phi/c^2} - c^2 A^2 e^{2\Phi/c^2}$, $\chi := -g_{t\phi}/g_{\phi\phi} = c^2 A e^{2\Phi/c^2}/g_{\phi\phi}$ as the traditional frame dragging rotational speed, $e^{2\nu/c^2} = (g_{tt}g_{\phi\phi} - g_{t\phi}^2)/g_{\phi\phi}^2 = W^2/g_{\phi\phi}^2$, and $\mu = 2k - 2\Phi$.

The geometry is then coupled to a perfect, pressureless fluid which respects the symmetries of the spacetime i.e., without velocity dispersion in the r and z directions. The angular speed of rotation of the particles (namely, the stars and galactic gas) is thus uniquely defined at any point $\mathrm{d}\phi/\mathrm{d}t = \Omega(r, z)$. The four-velocity of the matter is expressed as

$$U^\mu \partial_\mu = \frac{\partial_t + \Omega\,\partial_\phi}{\sqrt{-H}}, \tag{6}$$

where $H(r, z)$ is a normalisation factor, so that $U^\mu U_\mu \equiv -c^2$, i.e.,

$$H = -e^{2\Phi/c^2}(1 - A\,\Omega)^2 + e^{-2\Phi/c^2}W^2\,\Omega^2/c^2, \tag{7}$$

and the energy–momentum tensor of the matter is given by

$$T_{\mu\nu} = c^2 \rho(r,z)\, U_\mu U_\nu. \tag{8}$$

In particular, the function $W(r,z)$ appearing in (5) and (7) can be identified under the dust hypothesis as

$$W(r,z) = r. \tag{9}$$

The full coupling between matter and geometry has been worked out by Geroch and Winicour [45–47] (see [44,48] for a review). EFE are solved by a hierarchy of quadratures, and it is found that $H = H(\eta)$ and $\Omega = \Omega(\eta)$, where $\eta(r,z)$ is a field defined over the whole spacetime (see Sect. 3.1 for its physical interpretation) and

$$c^2\, \mathrm{d}H = 2\,\eta\ \mathrm{d}\Omega. \tag{10}$$

Furthermore, the norm and inner product of the Killing vectors of the spacetime, with the remaining EFE yield

$$g_{tt} = c^2 \frac{r^2\,\Omega^2/c^2 - \left(H - \eta\,\Omega/c^2\right)^2}{-H}, \tag{11}$$

$$g_{t\phi} = \frac{\eta^2/c^2 - r^2}{-H}\,\Omega + \eta, \tag{12}$$

$$g_{\phi\phi} = \frac{r^2 - \eta^2/c^2}{-H}, \tag{13}$$

$$\mu_{,r} = \frac{g_{tt,r}\,g_{\phi\phi,r} - g_{tt,z}\,g_{\phi\phi,z} - g_{t\phi,r}^2 + g_{t\phi,z}^2}{2c^2\,r}, \tag{14}$$

$$\mu_{,z} = \frac{g_{tt,z}\,g_{\phi\phi,r} - g_{tt,r}\,g_{\phi\phi,z} - 2\,g_{t\phi,z}\,g_{t\phi,r}}{2\,c^2 r}. \tag{15}$$

Moreover, the trace of the EFE gives

$$8\pi G e^{\mu/c^2}\rho = \frac{\eta_{,r}^2 + \eta_{,z}^2}{4\eta^2 r^2}\left[\eta^2\left(2 - \eta\ell(\eta)\right)^2 - c^4 r^4 \ell(\eta)^2\right], \tag{16}$$

where $\ell = (dH/d\eta)/H$. Finally, by requiring the integrability of (14) and (15) (which is equivalent to requiring the integrability of the equations of motion for the dust particle in circular orbits) we find that the entire class of solutions is fully determined by a choice of H, and a solution of the homogeneous Grad–Shafranov equation [27–29]

$$\tilde{\eta}_{,rr} - \frac{1}{r}\tilde{\eta}_{,r} + \tilde{\eta}_{,zz} = 0, \tag{17}$$

where

$$\tilde{\eta}(r,z) := \eta + \frac{c^2}{2} r^2 \int \frac{1}{\eta}\frac{\mathrm{d}H}{H} - \frac{1}{2}\int \frac{\eta}{H}\ \mathrm{d}H. \tag{18}$$

The linear partial differential equation (PDE) (17) can be put explicitly in terms of the field η. This gives the nonlinear PDE

$$\left(\eta_{,rr} - \frac{1}{r}\eta_{,r} + \eta_{,zz}\right)\left(2 - \eta\ell(\eta)\right) + \left(\eta_{,r}^2 - \eta_{,z}^2\right)\left[\ell'(\eta)\left(\frac{r^2}{\eta} + \eta\right) - \ell(\eta)\left(1 + \frac{r^2}{\eta^2}\right)\right] + r^2\frac{\ell(\eta)}{\eta}\left(\eta_{,rr} + \frac{3}{r}\eta_{,r} + \eta_{,zz}\right) = 0. \tag{19}$$

Thus, (19) uniquely determines $\eta(r,z)$ once a strictly negative $H(\eta)$ and $\eta(r,0)$ – or $\eta(0,z)$ – are arbitrarily assigned. From here on out, we refer to this class of solutions – whose every realisation is entirely defined by the arbitrary choice of two functions of one variable – as the (η, H) class.

The mathematical problem is then completely set by imposing Minkowskian boundary conditions at spatial infinity. Asymptotic Minkowskianity is a strong requirement to impose on the EFE solutions. Only ten curvature components, $R_{\mu\nu}$, enter into the EFE, whilst the imposed boundary conditions furnish twenty independent conditions – $R_{\mu\nu\rho\sigma} \longrightarrow 0$ at spatial infinity. However, prompted by the results on vacuum spacetimes in linearised GR [49] – which does provide a correct description of the asymptotic geometry far away from the matter content – we hold the view that imposing asymptotic Minkowskianity represents a valid boundary condition for the mathematical problem. Hence, in this work, we consider as physically relevant full GR galaxy models those solutions which satisfy the condition of asymptotic Minkowskianity.

3.1 Relevant observers and observed speed

In the first line of (5), the metric is written in the Zero Angular Momentum Observer (ZAMO) tetrad [19,21,27,29]

$$e^0 = \frac{r}{\sqrt{g_{\phi\phi}}}\,\mathrm{d}t, \quad e^1 = \sqrt{g_{\phi\phi}}\,(\mathrm{d}\phi - \chi\,\mathrm{d}t), \quad e^2 = e^{\mu/2c^2}\,\mathrm{d}r, \quad e^3 = e^{\mu/2c^2}\,\mathrm{d}z. \tag{20}$$

ZAMO is a natural observer for such spacetimes. Indeed, we can calculate the speed of the matter content according to ZAMO, which we call v_{Z}. This is given by

$$(e^0)_\mu U^\mu = \frac{1}{\sqrt{1 - \eta^2/r^2c^2}} = \gamma_{\mathrm{Z}} := \frac{1}{\sqrt{1 - v_{\mathrm{Z}}^2/c^2}} \Rightarrow \eta(r,z) = r\,v_{\mathrm{Z}}. \tag{21}$$

Thus, ZAMOs allow for a physical interpretation of the η field, namely, the product of the coordinate r by v_{Z}. Nonethe-

less, ZAMOs are just a realisation of the larger class of interesting observers for such spacetimes, whose coordinate lines are given by (t, ϕ), i.e., by the Killing vectors of the metric. In particular, we label "Killing observers" those defined by $U^{\mu}_{\rm K} := e^{-\Phi/c^2}\partial_t$. In general, Killing observers and ZAMOs do not measure the same physical quantities. This difference, arises from $\chi(r, z)$, the angular rotation speed of ZAMO with respect to the Killing vectors. We will call χ the dragging rotation speed from now on. This definition can be appreciated by calculating

$$\gamma_{\rm Z}\, v_{\rm Z} = (e^1)_{\mu} U^{\mu} \Rightarrow -H\, \gamma_{\rm Z}^2\, \frac{v_{\rm Z}}{r} = \Omega - \chi. \tag{22}$$

Equation (22) naturally prompts us to define the angular speed measured by ZAMOs, $\omega_{\rm Z} := v_{\rm Z}/r$. As we consider a low-velocity régime, the speed $v_{\rm Z}$ is sub-relativistic, and the Lorentz factor $\gamma_{\rm Z} = 1+\mathcal{O}(v_{\rm Z}^2/c^2)$ is negligible. The minus H factor can be neglected as we read from (7) that it is essentially the time-time component of the metric (plus a small $\mathcal{O}(v_{\rm Z}^2/c^2)$ term) and we expect the metrics under considerations to not possess a strong pseudo-Newtonian potential Φ.

In its approximated version, $\omega_{\rm Z} \approx \Omega - \chi$, Eq. (22) shows that the difference between physical quantities measured by ZAMO or by the Killing observer, are directly proportional to χ. Indeed, under the same hypothesis, we can define the speed $v_{\rm K} := r\,\Omega$ as the one measured by the Killing observers [21,27,29], as well as the dragging speed $v_{\rm D} := r\chi$. These are related by

$$v_{\rm K} - v_{\rm D} = -H\, \gamma_{\rm Z}^2\, v_{\rm Z} \approx v_{\rm Z}. \tag{23}$$

Naturally, the question arises of which of the theoretically measured velocity profiles – the one measured by ZAMOs, by the Killing observers, or by another class altogether (such as dust observers) – should be interpreted as the one measured in astronomical observations.

This highly non-trivial question depends on the very nature of the observed quantities by which the rotation curve velocity is inferred. When the observational speed is derived from a scan of the redshift z field of the matter in a distant galaxy, then it is the predicted $v_{\rm K}$ which should be compared with the plotted rotation curves – as discussed in [21,27,29], and contrary from what was supposed in [14–16]. In particular, we point out that this view is informed by a result dependent on only two factors: (i) our identification as local asymptotic Minkowskian observers for a distant galaxy; and (ii) on the validity of (6) in locally describing the dust four-velocity in the galaxy. However, the situation is starkly different when considering measurements carried out for the MW by the GAIA satellite, as in [17,26]. GAIA performs both radial redshift and proper motion measurements for the stars in the MW. Thus, the rotation speed inferred from the GAIA data is obtained from a mix of redshift and geometrical measurements. For this case, as discussed in [17,26] by Crosta and colleagues, ZAMO represents a valid observer for such data.

3.2 Rigidly rotating solutions

The general metric describing the subclass of vSB solutions i.e., rigidly rotating solutions, is obtained by imposing

$$\Omega(\eta) := 0 \Rightarrow H(\eta) := -1. \tag{24}$$

The line element is thus

$$\begin{aligned} {\rm d}s^2 = &- c^2\, \gamma_{\rm Z}^2\, {\rm d}t^2 + \left(\frac{r}{\gamma_{\rm Z}^2}\, {\rm d}\phi - v_{\rm Z}\, {\rm d}t\right)^2 \\ &+ e^{\mu/c^2}({\rm d}r^2 + {\rm d}z^2). \end{aligned} \tag{25}$$

Equations (11)–(16) become

$$g_{tt} = -1, \tag{26}$$

$$g_{t\phi} = \eta = r\, v_{\rm Z}, \tag{27}$$

$$g_{\phi\phi} = r^2 - \eta^2/c^2 = \frac{r^2}{\gamma_{\rm Z}^2}, \tag{28}$$

$$\mu_{,r} = -\frac{\eta_{,r}^2 - \eta_{,z}^2}{2c^2 r}, \tag{29}$$

$$\mu_{,z} = -\frac{\eta_{,r}\eta_{,z}}{2c^2 r}, \tag{30}$$

$$8\pi G e^{\mu/c^2}\rho = \frac{\eta_{,r}^2 + \eta_{,z}^2}{r^2}, \tag{31}$$

and (19) turns into the linear PDE

$$\eta_{,rr} - \frac{1}{r}\,\eta_{,r} + \eta_{,zz} = 0. \tag{32}$$

In particular, the general solution to (32) that can satisfy the chosen boundary conditions is given by

$$\begin{aligned} \eta(r, z) = \eta_c + \int_0^{+\infty} &\lambda\, {\rm d}\lambda r\, K_1(r\lambda)\, [A(\lambda)\cos(\lambda z) \\ &+ B(\lambda)\sin(\lambda z)] = \eta_c + \hat{\eta}(r, z), \end{aligned} \tag{33}$$

where $K_1(r\lambda)$ is the MacDonald function of the first order, $A(\lambda)$ and $B(\lambda)$ are the spectral densities for the even and odd modes of the solution, respectively, and η_c is the constant of integration.

4 Topological defects in Newtonian galaxy models

Before studying topological defects in full GR models of galaxies, care should be taken to verify their possible impact on Newtonian models. In the Newtonian limit of GR the line element for a stationary, axisymmetric geometry takes the form [50]

$$\begin{aligned} \mathrm{d}s^2 = &- c^2\left(1+\frac{2\Phi}{c^2}\right)\mathrm{d}t^2 + \left(1-\frac{2\Phi}{c^2}\right) r^2\,\mathrm{d}\phi^2 \\ &+ \left(1-\frac{2\Phi}{c^2}\right)\left(\mathrm{d}r^2+\mathrm{d}z^2\right), \end{aligned} \tag{34}$$

where $\Phi = \Phi(r, z)$ is the Newtonian potential defined by the matter distribution within the disc galaxy. For the geometry depicted by (34) the condition (4) is equivalent to

$$\lim_{r\to 0}\sqrt{\frac{g_{\phi\phi}}{r^2 g_{rr}}} = 1. \tag{35}$$

However, from (34) and (35) we can see that the condition to avoid topological structures within Newtonian disc galaxy models is automatically satisfied. Thus, we conclude that the presence of topological defects within general relativistic galaxy models would be a defining feature, without a direct Newtonian analogue. It would then represent a novel example of how GR and Newtonian gravity can develop important differences even in the weak-field regime.

5 Topological defects in rigidly rotating galaxy models

To investigate the topological structure of physically relevant solutions in the vSB subclass, we must start by enforcing asymptotic Minkowskianity on metric (25). From (27) and (33) we obtain the constraint

$$\eta_c = 0. \tag{36}$$

Then, by use of (29) and (30) we can write

$$\mu(r,z) = -\frac{1}{2c^2 r}\int_0^z \eta_r(r,z')\,\eta_{z'}(r,z')\,\mathrm{d}z' + F(r) + \mu_c, \tag{37}$$

where $F(r)$ must be chosen so that (29) is satisfied, and μ_c is the integration constant. To satisfy asymptotic Minkowskianity, and considering (33), we must then impose

$$\mu_c = -\lim_{r\to\infty} F(r). \tag{38}$$

We point out that (36) and (38) fix all the degrees of freedom of the solutions in terms of integration constants.

We are now in the position to investigate the presence of topological singularities in physically sound vSB solutions. By (5), we see that for the (η, H) class (4) becomes

$$\lim_{r\to 0} r^{-1} e^{(\Phi-k)/c^2}\sqrt{e^{-2\,\Phi/c^2}r^2 - e^{2\,\Phi/c^2}c^2A^2} = 1. \tag{39}$$

(39) can also be directly read in terms of metric components as

$$\lim_{r\to 0}\left(\frac{g_{\phi\phi}}{r^2\,g_{rr}}\right)^{1/2} = 1, \tag{40}$$

which for the vSB subclass becomes

$$\lim_{r\to 0} r^{-1} e^{-\mu/2\,c^2}\sqrt{r^2-\eta^2/c^2} = 1. \tag{41}$$

We want to use (41) to study the presence of conical singularities in vSB solutions. To begin, from (33), (36), and the expansion formula for the modified Bessel function [51] we get

$$\begin{aligned} \eta(r,z)_{|r\ll 1} &= \int_0^\infty \left[A(\lambda)\,\cos(\lambda z) + B(\lambda)\,\sin(\lambda z)\right]\mathrm{d}\lambda \\ &\quad + \left[\int_0^\infty \left[A(\alpha)\,\cos(\alpha z) + B(\alpha)\,\sin(\alpha z)\right]\alpha^2\,\mathrm{d}\alpha\right] \\ &\quad \cdot r^2\log(r) - \gamma\left[\int_0^\infty \left[A(\beta)\,\cos(\beta z)\right.\right. \\ &\quad \left.\left. + B(\beta)\,\sin(\beta z)\right]\beta^2\,\mathrm{d}\beta\right] r^2 + \mathcal{O}(r^3) \\ &=: \sum_{n=0}^\infty a_n z^n + \left(\sum_{n=0}^\infty b_n z^n\right) r^2\,\log(r) - \gamma \\ &\quad \times \left(\sum_{n=0}^\infty b_n z^n\right) r^2 + \mathcal{O}(r^3) \\ &=: G(z) + H(z)\,r^2\,\log(r) - \gamma\,H(z)\,r^2 + \mathcal{O}(r^3), \end{aligned} \tag{42}$$

where γ is the Euler–Mascheroni constant, and we have defined

$$a_n := \begin{cases} \left[(-1)^n/n!\right]\int_0^\infty A(\lambda)\,\lambda^n\,\mathrm{d}\lambda & n = 2k,\ k\in\mathbb{N}, \\ \left[(-1)^n/n!\right]\int_0^\infty B(\lambda)\,\lambda^n\,\mathrm{d}\lambda & n = 2k+1,\ k\in\mathbb{N}, \end{cases} \tag{43}$$

and

$$b_n := \begin{cases} \left[(-1)^n/n!\right]\int_0^\infty A(\alpha)\,\alpha^{n+2}\,\mathrm{d}\alpha & n = 2k,\ k\in\mathbb{N}, \\ \left[(-1)^n/n!\right]\int_0^\infty B(\alpha)\,\alpha^{n+2}\,\mathrm{d}\alpha & n = 2k+1,\ k\in\mathbb{N}. \end{cases} \tag{44}$$

We notice that $G(z) = const = k$ cannot be realised as it would imply

$$0 = G(z) - k = \sum_{n=0}^{\infty} a_n z^n - k$$
$$= \sum_{n=0}^{\infty} (a_n - k) z^n = 0 \Rightarrow a_n = k \ \ \forall n \in \mathbb{N}, \tag{45}$$

where the last condition cannot be achieved for any non-trivial choice of $A(\lambda)$ and $B(\lambda)$, as can be seen from (43). The same reasoning also shows that $H(z) = const$ is not a possibility. Therefore, $g_{\phi\phi}$ is a function of z near the axis of symmetry, namely

$$\lim_{r \longrightarrow 0} g_{\phi\phi}(r, z) = -\left[G(z)\right]^2 . \tag{46}$$

To understand if (41) can be satisfied, we also need to gauge the behaviour of $g_{rr}(r, z)$, and thus of $\mu(r, z)$ near the rotation axis. From (42) we get

$$\eta_{,r}(r, z)\big|_{r \ll 1} = H(z) \left[1 - 2\,\gamma + 2\,\log(r)\right] r \, + \mathcal{O}(r^2), \tag{47}$$

$$\eta_{,z}(r, z)\big|_{r \ll 1} = \frac{\mathrm{d}G(z)}{\mathrm{d}z} + \frac{\mathrm{d}H(z)}{\mathrm{d}z} \left[\log(r) - \gamma\right] r^2 + \mathcal{O}(r^3), \tag{48}$$

From (37), (47) and (48) we obtain

$$\begin{aligned} \mu(r, z)\big|_{r \ll 1} &= \frac{1}{c^2} \left[\gamma - \frac{1}{2} - \log(r)\right] \int_0^z \frac{\mathrm{d}G(z')}{\mathrm{d}z'} H(z') \, \mathrm{d}z' \\ &\quad + F(r)\big|_{r \ll 1} + \mu_c + \mathcal{O}(r) \\ &=: M(z) + N(z) \, \log(r) + F(r)\big|_{r \ll 1} \\ &\quad + \mu_c + \mathcal{O}(r), \end{aligned} \tag{49}$$

where $M(z)$ and $N(z)$ are forced to be non-constant – as already discussed for $G(z)$ and $H(z)$. (49) shows that any vSB metric, that is not pathological at spatial infinity, is bound to become singular near the rotation axis. From the choice of the spectral densities in (33), this pathological behaviour can be avoided for specific sets of values of z – as in the original BG model [16] – but cannot be completely removed. Nonetheless, from (46) and (49) it is now clear that (40) cannot be satisfied by the EFE solutions under study. Hence, asymptotically Minkowskian vSB solutions necessarily display the presence of quasi-regular singularities.

As discussed in Sect. 1, we could sidestep the problematic feature of curvature singularities in a galaxy model invoking the local nature of GR, if these singularities are present only in the would-be bulge region or far away from the thin disc (see [17,26,32]). However, the presence of topological defects directly impacts the global geometry of these spacetimes. The very definition of the chosen physical coordinates must be put under scrutiny, especially if these solutions are to be compared to the standard Newtonian ones, and observational data. In GR, coordinates are a priori devoid of a physical meaning. They acquire one only when a measurement procedure is defined.

The impact of conical singularities on the definition of the angle coordinate for physical observers inside a vSB dust cloud must be correctly addressed when using such models. In particular, the topological singularity can always be negated on a given plane – e.g., the equatorial one – by a proper choice of the spectral densities and of μ_c. Indeed, given $A(\lambda)$ and $B(\lambda)$ which allow for

$$\lim_{r \longrightarrow 0} \mu(r, 0) = \mu_0 + \mu_c = \mu_\infty + \mu_c = \lim_{r \longrightarrow 0} \mu(r, 0), \tag{50}$$

it would be possible to define

$$\mu_c = -\mu_\infty = -\mu_0. \tag{51}$$

Thus eliminating on the equatorial plane the topological singularity, whilst maintaining the proper boundary conditions. It is precisely this choice that a physical observer would take, given a specific vSB realisation. However, such a choice, which validates the angular coordinate's common physical meaning, fixes a degree of freedom of the model. Therefore, any physical quantity calculated will be directly impacted by this choice – i.e., density and any kind of rotation curve calculations, should only be carried out once the coordinate choice has been defined in a physically sound way. For example, the μ_c fixing procedure employed in [16] to estimate the amount of DM which can be explained away by the BG model, would need to be revised, since μ_c should be picked to eliminate the topological defect otherwise present in the solution.

The presence of topological singularities cannot be avoided, except in isolated planes. Therefore, any vSB model that respects the chosen boundary conditions defines a spacetime with a highly non-trivial topology. Non-isolated 2D spacetime slices of the type $\{t = const, z = const\}$ harbour conical singularities in $r = 0$. However, unlike more well-known cases, e.g., standard cosmic strings, the conical structure is more complex, as can be seen by the z dependence in the Eqs. (13) and (49). The resulting global geometrical structure of vSB spacetimes can be obtained by slicing the solution near the rotation axis along 2D surfaces of the type $z = const$, and folding each one in a cone with a varying angle of identification α. Indeed, the resulting topological structure can be seen as generated by the presence of an exotic cosmic string with a mass per unit length varying along its extension. Figure 1 shows a tentative visualisation of the resulting geometry.

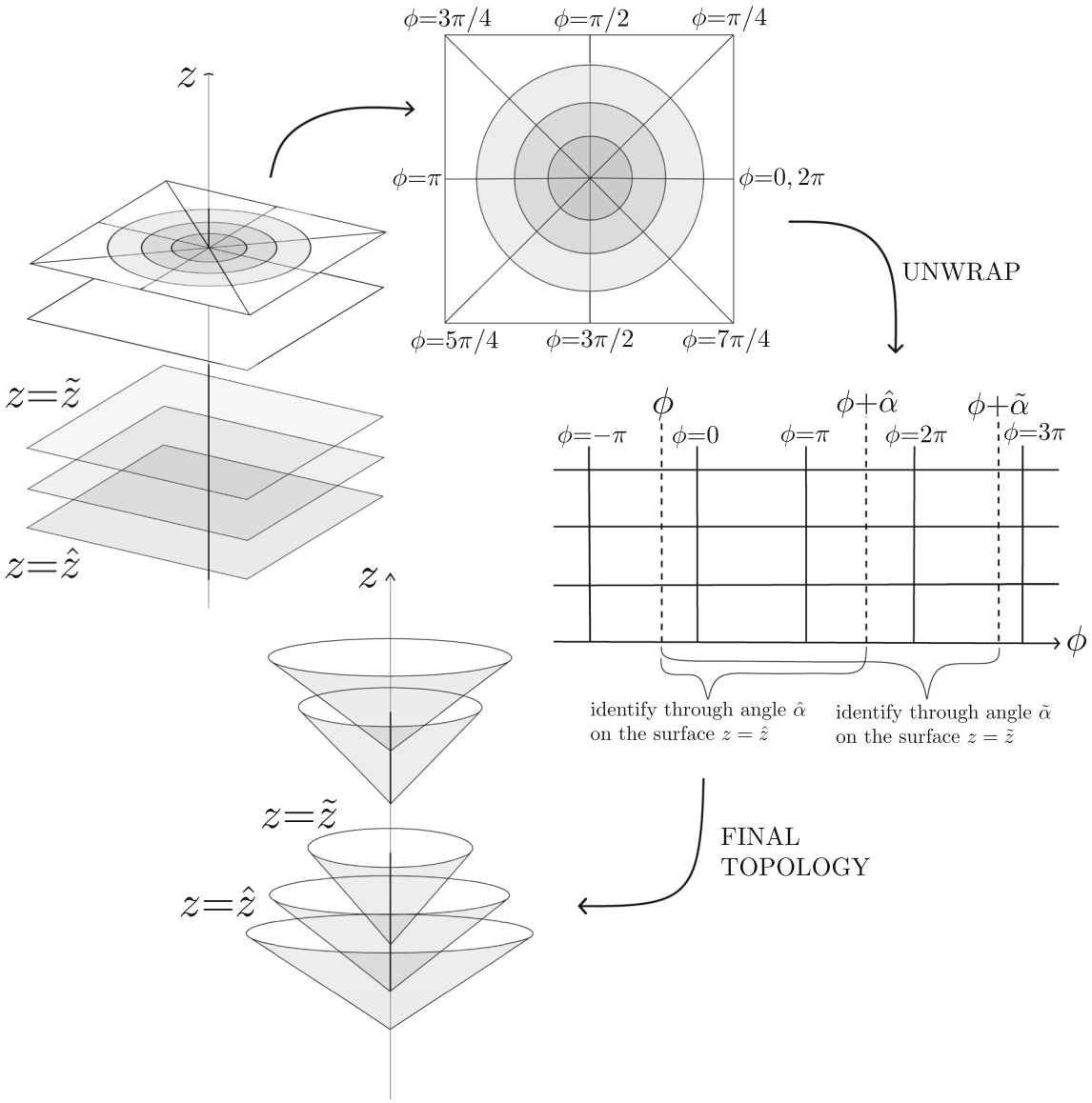

Fig. 1 Resulting geometry around the z-axis of a vSB asymptotically Minkowskian solution. The slicing and identification procedure is shown for different constant values of z

6 Impact of topological defects in the Balasin–Grumiller galaxy model

We have proven the presence of topological defects within the vSB spacetimes. We can now further study their impact in the special realisation of the BG model, defined by the choice for η of

$$\eta_{\rm BG}(r,z) = V_0(R-r_0) + \frac{V_0}{2}\sum_{\pm}\left(\sqrt{r^2+(z\pm r_0)^2} - \sqrt{r^2+(z\pm R)^2}\right), \tag{52}$$

where V_0 is the flat-regime velocity of the galaxy rotation curve, R is the galaxy radius and r_0 is the bulge radius.

6.1 The Milky Way rotation curve: fit to GAIA DR3 data

As discussed in Sect. 1, BG represents the first fully general relativistic disc galaxy model to be empirically tested in the fitting of data. Indeed, Crosta and colleagues [17,26] have shown that the model provides accurate fits to the rotation curve of the Milky Way extracted by the DR3 GAIA data.

By modelling the Galaxy via the BG model we neglect the bugle contribution to the average dynamics. We are considering a disc approximation to its baryonic structure. This approach cannot fully capture the rotation curve behaviour near the galactic centre, in which the bulge and the central galactic black hole play an important role [52–55]. Furthermore, we are not directly considering the spherical DM halo.

A GR modelling of the disc, and of the halo itself, could lead to fairly different properties of the halo w.r.t. the ones inferred in the conventional Newtonian approach (see, e.g., [27,28,56]). As addressing such changes, and their influences on the galactic dynamics, goes beyond the scope of this paper, we refer it to future work.

In the data fitting procedure of [17,26], the authors disregarded the coordinate dependence of the $\mu(r,z)$ field and kept it as a constant, i.e., $\mu(r,z) \approx \bar{\mu}$, on account of $\mu \propto (V_0/c)^2 \ll 1$. Although this choice might be justified by the expected small value of $\mu(r,z)$, the authors did not consider the relevance of $\mu(r,z)$ in determining the presence of topological pathologies. Indeed, in [17,26] the value of $\bar{\mu}$ is left as a free parameter. However, even if we were to consider the BG as a viable solution exclusively for the thin disc within the galactic plane (and for a limited radius, see [24]), we still would need to exercise care in dealing with topological defects.

Here, we perform data fitting over DR3 GAIA data whilst accounting for the functional form of the field μ on the equatorial plane, and while removing any topological defect on said plane. From, (29) and (52) we obtain (for $r_0 \neq R$, i.e., the only physical case)

$$\mu_{\rm BG}(r,0) = \mu_c - \frac{V_0^2}{2c^2}\left(\frac{1}{2}\log(1+\frac{r^2}{r_0^2}) + \frac{1}{2}\log(1+\frac{r^2}{R^2}) - \operatorname{arcsinh}\left(\frac{2r^2+R^2+r_0^2}{R^2-r_0^2}\right)\right). \tag{53}$$

Thus, from (53) we see that to avoid topological defects on the plane we must impose

$$\mu_c = -\frac{V_0^2}{2c^2}\operatorname{arcsinh}\left(\frac{R^2+r_0^2}{R^2-r_0^2}\right). \tag{54}$$

We employ the data set named "ALL" in [26] to conduct our analysis. This data set is constituted by 719143 stars including 241918 OBA stars, 475520 RGB giants, and 1705 Cepheides on near-circular orbits. These stars have been selected to have a proper disc height below 1 kpc, thus within the MW thin disc. All the stars in the sample have a distance from the galactic centre, r, of $4.5\,\text{kpc} < r < 19\,\text{kpc}$, where the lower-end bound was selected to avoid the impact of the spiral arms on the dynamic traced by the stars. The "ALL" sample is then binned in cylindrical rings as a function of the distance from the axis of rotation, using Knuth's Rule [57] for the optimal choice of the bin size (≈ 0.1 kpc in this case). For a more in depth description of the data set, see Section 3 and Appendix A of [26].

To fit BG to the data, we employ a Monte Carlo Markov Chain approach (MCMC) based on the Affine Invariant Ensemble Sampler (AIES) implemented in the python library EMCEE [58]. To explore the parameter space, we implement the same log likelihood function as in [17,26], i.e.,

$$\log\mathcal{L} = -\frac{1}{2}\sum_{i=1}^{N}\left[\frac{\left[V_\phi(r_i) - V_\phi^{\rm BG}(r_i|\boldsymbol{\theta})\right]^2}{\sigma^2_{V_\phi,i}} + \log\left(2\pi\sigma^2_{V_\phi,i}\right)\right] - \frac{1}{2}\left[\frac{\left[\rho_{bar}(r_\odot) - \rho^{\rm BG}(r_\odot|\boldsymbol{\theta})\right]^2}{\sigma^2_{\rho_{bar,\odot}}} + \log\left(2\pi\sigma^2_{\rho_{bar,\odot}}\right)\right], \tag{55}$$

where N is total number of bin in the data set (i.e., 128 in this case), V_ϕ represents the median rotational velocity of the stars in the i-th bin, $\sigma_{V_\phi,i}$ are their respective errors, $\rho_{bar}(r_\odot)$ is the measured baryons density at the Sun distance from the galactic centre ($r_\odot \approx 8.249$ kpc) and $\sigma_{\rho_{bar,\odot}}$ is its estimated error, which are taken to be 0.084 $M_\odot$/kpc^3 and 0.012 $M_\odot$/kpc^3, respectively [26,59]. The quantities with the suffix BG indicate the expected value for the BG model defined by the parameters $\boldsymbol{\theta} = (V_0, R, r_0)$, at the given distance on the galactic plane. Notice that our list of parameters does not include $\bar{\mu}$ (indicated as ν_0 in [17,26]), as we consider the functional form of μ and μ_c is fixed to eliminate the topological singularity on the galactic plane. As priors over the free parameters, V_0, R, r_0 we implement the same Normal distributions used in [26], i.e.,

a. $\mathcal{N}(\bar{x} = 263, \sigma = 50)$ km/s for V_0, (56)

b. $\mathcal{N}(\bar{x} = 48, \sigma = 50)$ km/s for R, (57)

c. $\mathcal{N}(\bar{x} = 0.2, \sigma = 4)$ kpc for r_0. (58)

The MCMC has been run with 50 chains for a million steps each, a burn-in phase of 5000 steps and a thinning parameter of 10. In Fig. 2 we report the curve of best fit and the related

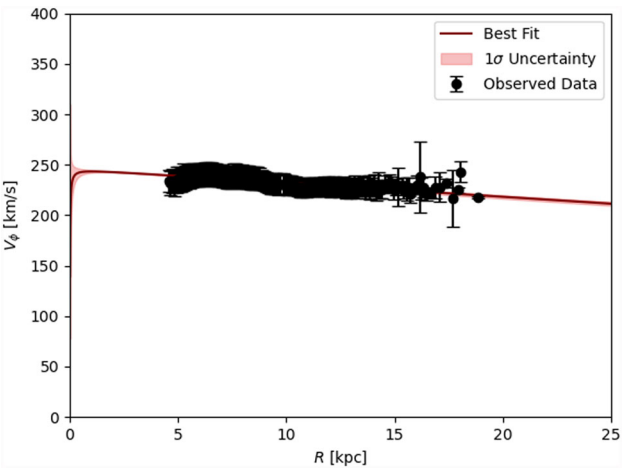

Fig. 2 Best fit curve to the GAIA DR3 sample and related one σ uncertainty interval

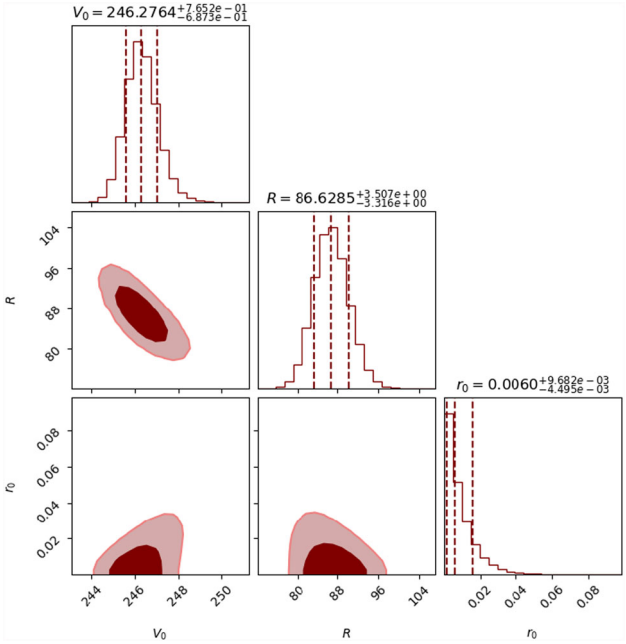

Fig. 3 Posterior distribution for the BG parameters, i.e., V_0, R, and r_0

one σ uncertainty interval. In Fig. 3 we show the posterior distribution obtained by the MCMC analysis.

In Table 1 we report the obtained values for the fit parameters, and their uncertainties, as well as the respective density at the sun distance. Moreover, we display the results obtained by Beordo and colleagues in [26] for direct comparison.

The obtained results for V_0, R and r_0 are compatible with the ones found in [26]. However, we notice that the value of r_0 still reduces significantly w.r.t. the previous value, and it is compatible with the latter only due to its large error. Moreover, we note that the effective bulge radius of the topologically safe BG realisation in Table 1 is at odds with values present in the literature and obtained via standard Newtonian models, e.g., [52] with $r_0 = 0.12 \pm 0.01$, and $r_0 = 0.87 \pm 0.07$ in [53]. At the same time, it agrees with other recent results for detailed mass modelling of the Galaxy [26], although with a systematically lower value. Such a situation can be expected, given the approximation employed in our study and the difficulties in disc galaxies mass modelling [26,39,52,53,60,61]. On the other hand, we find that the overall extension of the Galaxy, exemplified by R in BG, is in agreement with the expectations [26,39,52,53]. However, once we have fixed the BG realisation to be topologically safe, i.e., devoid of conical singularities in the origin, the value of the estimated density at $r_\odot$ drops drastically, remaining compatible with the observed value only at a 3σ level. This would suggest that a topologically safe BG model cannot represent a good fit to both the GAIA DR3 rotation curve and the observed local baryonic density at the Sun's position [59]. However,

Table 1 Best fit parameters and related uncertain for the topologically safe fit of BG to the GAIA DR3 sample ALL and the corresponding values found in Beordo et al. [26]

	Topological safe fit	Fit Beordo et al. [26]
V_0 [km/s]	$246.2^{+0.7}_{-0.7}$	256^{+10}_{-7}
R [kpc]	86^{+4}_{-3}	71^{+13}_{-11}
r_0 [kpc]	$0.006^{+0.009}_{-0.004}$	$0.2^{+0.18}_{-0.12}$
Exp[$\bar{\mu}$]	Fixed by topology	$0.087^{+0.017}_{-0.012}$
$\rho_\odot^{BG}$ [$M_\odot$/pc^3]	$0.027^{+0.005}_{-0.004}$	$0.08^{+0.012}_{-0.012}$

it is still possible to modify the log likelihood in (55) to further penalise divergences from the observed local baryonic density and re-estimate the parameters. Nonetheless, such a procedure would necessarily worsen the fit of the rotation curve.

6.2 Gravitational lensing: angle of deflection

We have shown that eliminating the topological singularity changes the values obtained for BG by fitting the same GAIA DR3 sample as [26]. Unfortunately, we have found that the impact of these changes is not statistical significant with the current observational resolution. However, another observable which can be used to gauge the impact of topological singularities in BG is the angle of deflection expected for strong gravitational lensing by the disc galaxy modelled.

Here, we follow [24] and reproduce the calculation of the equatorial lensing of an edge-on spiral galaxy, i.e., the so-called "disc configuration" [62], for the realisations of the BG model presented in [26], and the one produced by our own fit of the GAIA DR3 data, devoid of topological singularities on the plane.

The deflection angle, α, for an observer-lens-source system separated by cosmological distances (i.e., Gpc), and aligned along the line of sight, is well-approximated away from the bulge by (see Eqn. (69) of [24], and the paper for an in-depth derivation.)

$$\alpha = \frac{1}{2}\left(\frac{V_0}{c}\right)\left(\frac{R^2}{b^2} - \frac{r_0^2}{b^2}\right)\int_{\phi_S}^{\phi_O} |\cos\phi|\, \mathrm{d}\phi + \mathcal{O}\left(\left(\frac{V_0}{2}\right)^2\right), \tag{59}$$

where b is the impact parameter of the light ray, and $\phi_S = 0$ and $\phi_O = \pi$ are the angular coordinates of the source and of the observer, respectively.

However, the identification $\phi_S = 0$, and $\phi_O = \pi$ is only valid if $\phi \in [0, 2\pi]$. If the spacetime presents a topological singularity on the equatorial plane, as for the BG realisation reported in [26], we should take into account the angle defect and adjust the value of ϕ_O accordingly. In particular,

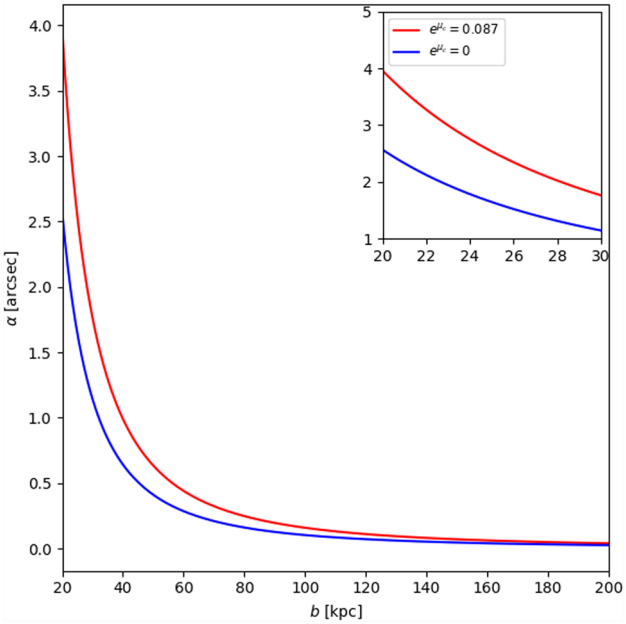

Fig. 4 Bending angle curves, as a function of the impact parameter, for the BG realisations of the Milky Way obtained by fitting the GAIA DR3 data and from the parameters reported in [26]

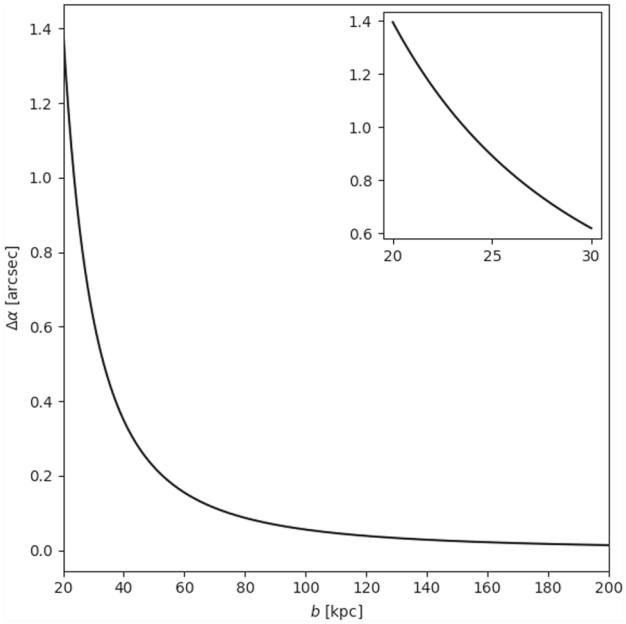

Fig. 5 Differences between the bending angles derived for the two realisations of the BG model of the Milky Way (previous fitting of [26] and the obtained topologically safe model)

as $\eta_{\rm BG}(r,0) \propto r^2$ for $r \ll 1$, we see that the BG line element on the equatorial plane can be approximated by

$$ds^2_{BG|r\ll 1} \approx -dt^2 + r^2\, d\phi^2 + e^{\mu_0}\left(dr^2 + dz^2\right). \tag{60}$$

Equation (60) can recast in the canonical form of (3) by the coordinate transform $r \to \hat{r} = e^{\mu_c/2} r$, $z \to \hat{z} = e^{\mu_c/2} z$, giving

$$ds^2_{BG|r\ll 1} \approx -dt^2 + e^{-\mu_0}\hat{r}^2\, d\phi^2 + d\hat{r}^2 + d\hat{z}^2, \tag{61}$$

where in analogy to (3) we can identify $f = e^{-\mu_0/2}$, so that the range spanned by the angle ϕ is actually $\phi \in \left[0, 2\pi e^{-\mu_0/2}\right]$. Now, for the configuration of interest, we can generalise Eq. (59) to account for the presence of a conical singularity on the plane, i.e.,

$$\alpha = \frac{1}{2}\left(\frac{V_0}{c}\right)\left(\frac{R^2}{b^2} - \frac{r_0^2}{b^2}\right)\int_0^{f\pi} |\cos\phi|\, d\phi + \mathcal{O}\left(\left(\frac{V_0}{2}\right)^2\right). \tag{62}$$

We can now calculate $\alpha(b)$ from Eq. (62) for both the realisations of BG with parameters reported in Table 1. In Fig. 4 we show the two curves obtained for the deflection angle corresponding to the best fit parameters, whilst in Fig. 5 we report the bending angle difference between the two curves.

The plots in Figs. 4 and 5 show that the presence of a topological singularity in the realisation of BG derived in [26] for the Milky Way leads to a larger bending angle than in the case of the topologically safe BG model. The BG model has been proven to produce physical bending angles for light rays grazing the galaxy [24] where BG was considered devoid of topological singularities a priori. As in [24] we find that the bending angle magnitude grows to unphysical values when we calculate it for light rays passing deep within the galactic disc, signalling a further problematic feature of BG, if taken as a global galaxy model. Moreover, we have shown that a difference of order unity in the bending angle can occur within the galaxy radius in the presence of topological defects. This shows once more that the correct consideration of the topological structure of such spacetimes directly impacts the calculations of physical observables within these models.

7 Topological defects in differentially rotating, pressureless galaxy models

We could question whether such topological pathologies, as well as curvature singularities, may be avoided when considering a larger class of EFE solutions to model average galaxy dynamics. In particular, we might ask whether dropping the assumption of rigid rotation – thus working in the (η, H) class – is sufficient to construct models devoid of such pathologies, or if an effective internal pressure must be added to the system to achieve this goal.

Let us then consider the (η, H) class. As discussed in Sect. 3, the general solution for this class is entirely iden-

tified by the choice of two one-variable functions: (i) $H(\eta)$ and $\eta(r,0)$ (or $\eta(0,z)$); or (ii) $v_{\rm K}(r,0)$ and $v_{\rm D}(r,0)$ (or the respective on-axis quantities). This starkly contrasts with the vSB subclass, in which only the choice of an "initial" profile for $\eta(r,z)$ would define the whole solution. Thus, the differentially rotating solutions of the (η, H) class possess infinitely more degrees of freedom than the vSB models.

We can use the freedom allowed by the differential rotation to get rid of curvature singularities along the axis in the solutions. As discussed in [27], once we impose the sufficient, but not necessary, condition $v_{{\rm D},r}(0,z)=0$, the model has no curvature singularities along the rotation axis.

On the other hand, to obtain models devoid of topological singularities we require (see (13) and (40)) that

$$\lim_{r\longrightarrow 0} e^{\mu/2c^2}\sqrt{\frac{1-\eta^2/c^2}{-H(\eta)r^2}}=1 \Leftrightarrow \lim_{r\longrightarrow 0}\frac{e^{\mu/2c^2}}{\sqrt{-H(rv_Z)}\gamma_Z}=1, \tag{63}$$

where in the second relation we have used (21). Let us then assume that the field H is a regular function of η. We can thus write

$$H(rv_Z)=-1+\sum_{n=1}^{+\infty}c_n(rv_Z)^n, \tag{64}$$

where c_n are arbitrary coefficients. From (10) and (64) we then have

$$\Omega(rv_Z)=\Omega_0+\frac{c^2}{2}c_1\log(rv_Z)+\frac{c^2}{2}\sum_{n=2}^{+\infty}\frac{n}{n-1}c_n(rv_Z)^{n-1}. \tag{65}$$

From (65) we find that to meet the requirement of zero rotational velocity on the symmetry axis we must impose the constraints $c_1=0$ in (64) and $\Omega_0=0$ in (65). Therefore, we have

$$H(rv_Z)=-1+\sum_{n=2}^{+\infty}c_n(rv_Z)^n, \tag{66}$$

$$\Omega(rv_Z)=\frac{c^2}{2}\sum_{n=2}^{+\infty}\frac{n}{n-1}c_n(rv_Z)^{n-1}. \tag{67}$$

If we are now assuming the selected model of the (η, H) class to represent a physical galaxy, we have to require $v_Z/c\ll 1$, so that $\lim_{r\to 0} rv_Z(r,z)=0$. In particular, this certainly is realised if we impose the condition $v_Z(0,z)=0$, which we are free to do since we can arbitrarily pick the initial values of two of the three relevant velocities – i.e., v_Z, v_K and $v_{\rm D}$ – on an axis for a (η, H) model. Then, from (11)–(15), (66) and (67) it follows that

$$\lim_{r\longrightarrow 0}\mu_{,r}(r,z)=0, \tag{68}$$

$$\lim_{r\longrightarrow 0}\mu_{,z}(r,z)=0. \tag{69}$$

From (68) and (69) we can then fix $\mu(0,z)=0$, as we still have the freedom to choose an integration constant in the defining $\mu(r,z)$. Thus, for $v_Z(0,z)=0$, the model meets the regularity condition (63) and is devoid of conical singularities. Moreover, since we are still free to pick the profile of either $v_{\rm K}$ or $v_{\rm D}$ on the symmetry axis. Therefore, we can pick $v_{\rm D}$ so that the condition $v_{{\rm D},r}(0,z)=0$ for the absence of curvature singularities is also met. Thus, we find that the two conditions, which ensure the absence of curvature and topological singularities on the rotation axis, can be consistently enforced for the same solution of the (η, H) family.

We notice that recent work put forth a subclass of exact solution for differentially rotating dust spacetimes which results devoid of conical or curvature singularities along the z-axis [29]. This subclass of solutions of the (η, H) class displays asymptotic flatness at spatial infinity, in contrast with rigidly rotating models. This is possible due to the nonlinearities of Eq. (19), which brings about a regularisation of the solution at spatial infinity. However, these solutions can display local effective negative energy density beyond a fixed cylindrical radius – once more, a behaviour which has no Newtonian analogue. In [29], the authors interpret such behaviour as due to the gravitational binding energy of the galaxy, which must be accounted for in bounded systems , and it has to be negative. Nonetheless, an ulterior interpretation might be that such models breakdown outside the transition radius between positive and negative local energy density, i.e., they loose any physical applicability to real systems. In this case, as the subclass of solutions presented in [29] is the only subclass of (η, H) consistent with a low-energy limit description of a rotating dust system in GR, we should **(i)** look for matching conditions within the viability region of these solutions to an asymptotically flat vacuum metric, or **(ii)** conclude that only with the addition of an effective internal pressure even a local, piece-wise description of a galaxy is possible within GR. Both options represent monumental mathematical tasks which go beyond the scope of the current paper and are thus postponed to future work.

8 Conclusions and perspectives

In 1973 John Archibald Wheeler famously summarised General Relativity as: *Space tells matter how to move, matter tells space how to curve* [49], pointing to the geometrical nature of GR. Whilst GR describes spacetime as a four-dimensional

pseudo-Riemannian manifold where local geometry is everywhere defined by its matter-energy content through Einstein's Equations, it does not prescribe its global topological structure. Nonetheless, topological questions play a crucial role in our understanding of the Universe [63–70], since topology can *limit* possible matter content and plays a non-trivial role in defining physical coordinates.

Here we have used spacetime topology in this limiting fashion. Even at the level of modelling galaxies in full GR, topological consideration must be thoroughly studied. They can restrict the scale of viability of a model or rule it out entirely. Furthermore, they inform the choice of the coordinates used in the study of the spacetime.

In this paper, we have shown that asymptotically Minkowskian van Stockum–Bonner spacetimes – i.e., stationary, axisymmetric, rigidly rotating, dust solutions of Einstein's equations – are studded with topological singularities along the rotation axis. The presence of this network of non-isolated topological defects (see Fig. 1) constitutes a further pathological behaviour of such models, which impacts the global geometrical structure of the spacetimes and possesses no direct analogue in Newtnoian gravity.

In particular, the physical definition and interpretation of the angular coordinate is highly non-trivial. These issues can be avoided on isolated $z = const$ surfaces, such as the equatorial plane. However, doing so reduces the degree of freedom of the solutions. Hence, the estimation of physically relevant quantities, e.g., rotation curves and gravitational lensing, is affected by the conical singularities even though these are concentrated on the symmetry axis.

We gauged the impact of such pathologies for the Balasin-Grumiller model [16] on the fitting of the Milky Way rotation curve, following the previous works by Crosta and colleagues [17,26]. We showed that with the ulterior constraint given by the topological defect, the model cannot provide a good fit to both the GAIA DR3 rotation curve data and the local baryonic density. Thus, our results seem to disqualify the model as valid even locally in the Milky Way. Furthermore, we have proven the importance of considering the correct topological structure by showing its imprint over the gravitational lensing by the model. Indeed, we found that not considering the possible presence of conical singularities on the equatorial plane leads to differences of order unity in the deflection angle within the galaxy radius.

The (η, H) class investigated in [19–22,27–29] (which generalises the van Stockum–Bonner class), may prove to be a fruitful line of enquiry. By dropping the rigidity of the dust and allowing for differential rotation, this class of models is physically realistic. Moreover, we have shown that a solution devoid of both topological and curvature singularities can be selected within the class, with such an example actually presented in [29]. However, the inclusion of an effective internal pressure is still necessary to properly model the galactic bulge and vertical gravity within disc galaxies (see [30] for a first-order implementation of the pressure).

Therefore, the introduction of internal effective pressure in full GR galaxy modelling still remains a high priority. Nonetheless, we have shown the potential for topological considerations in model selection by further limiting the possible employment of van Stockum–Bonnor solutions in full GR modelling of galaxies, as well as in determining viability of models in the wider, differentially rotating class. We plan to make full use of these considerations in future work.

Acknowledgements The author would like to thank David Wiltshire, Sergio Cacciatori, Vittorio Gorini, Chris Harvey-Hawes, Morag Hills, Zachary Lane, Michael Williams, Federico Re and Emma Johnson for useful discussions. In particular, the author wishes to thank Morag Hills for providing the plot in Sect. 5.

Data Availability Statement This manuscript has no associated data. [Author's comment: Data sharing not applicable to this article as no datasets were generated or analysed during the current study.]

Code Availability Statement Code/software will be made available on reasonable request. [Author's comment: The code/software generated during and/or analysed during the current study is available from the corresponding author on reasonable request.]

Funded by SCOAP[3].

References

1. C. Will, Liv. Rev. Relativ. (2014). https://doi.org/10.12942/lrr-2014-4
2. R.C. Tolman, Phys. Rev. **55**, 364 (1939). https://doi.org/10.1103/PhysRev.55.364
3. J.R. Oppenheimer, G.M. Volkoff, Phys. Rev. **55**, 374 (1939). https://doi.org/10.1103/PhysRev.55.374
4. K. Schwarzschild, (1999). https://doi.org/10.48550/arXiv.physics/9905030. arXiv:physics/9905030
5. R.P. Kerr, Phys. Rev. Lett. **11**, 237 (1963). https://doi.org/10.1103/PhysRevLett.11.237
6. K. Akiyama et al., Astrophys. J. Lett. **875**(1), L1 (2019). https://doi.org/10.3847/2041-8213/ab0ec7
7. A. Einstein, Sitzungsberichte der Königlich Preussischen Akademie der Wissenschaften (1918), pp. 154–167
8. B.P. Abbott et al., Phys. Rev. Lett. **116**, 061102 (2016). https://doi.org/10.1103/PhysRevLett.116.061102
9. B. Mashhoon, (2008). https://doi.org/10.48550/arXiv.gr-qc/0311030. arXiv:gr-qc/0311030

10. M.L. Ruggiero, D. Astesiano, J. Phys. Commun. **7**(11), 112001 (2023). https://doi.org/10.1088/2399-6528/ad08cf
11. M. Bartelmann, Class. Quantum Gravity **27**(23), 233001 (2010). https://doi.org/10.1088/0264-9381/27/23/233001
12. L. Ciotti, Astrophys. J. **936**(2), 180 (2022). https://doi.org/10.3847/1538-4357/ac82b3
13. K. Glampedakis, D.I. Jones, Class. Quantum Gravity **40**(14), 147001 (2023). https://doi.org/10.1088/1361-6382/acdd4a
14. F.I. Cooperstock, S. Tieu, Int. J. Mod. Phys. A **22**(13), 2293 (2007)
15. F.I. Cooperstock, S. Tieu, Mod. Phys. Lett. A **23**(21), 1745 (2008)
16. H. Balasin, D. Grumiller, Int. J. Mod. Phys. D **17**, 475 (2008)
17. M. Crosta, M. Giammaria, M. Lattanzi, E. Poggio, MNRAS **496**, 2107 (2020)
18. G.O. Ludwig, Eur. Phys. J. C **81**(2), 186 (2021). https://doi.org/10.1140/epjc/s10052-021-08967-3
19. D. Astesiano, S.L. Cacciatori, V. Gorini, F. Re, Eur. Phys. J. C **82**(6), 554 (2022). https://doi.org/10.1140/epjc/s10052-022-10506-7
20. D. Astesiano, Gen. Relativ. Gravit. **54**(7), 63 (2022). https://doi.org/10.1007/s10714-022-02947-y
21. D. Astesiano, S.L. Cacciatori, M. Dotti, F. Haardt, F. Re, (2022). https://doi.org/10.48550/arXiv.2204.05143. arXiv e-prints arXiv:2204.05143
22. D. Astesiano, M.L. Ruggiero, Phys. Rev. D **106**, 044061 (2022). https://doi.org/10.1103/PhysRevD.106.044061
23. D. Astesiano, M.L. Ruggiero, Phys. Rev. D **106**, L121501 (2022). https://doi.org/10.1103/PhysRevD.106.L121501
24. M. Galoppo, S.L. Cacciatori, V. Gorini, M. Mazza, (2024). https://doi.org/10.48550/arXiv.2212.10290. arXiv:2212.10290
25. M.L. Ruggiero et al., Class. Quantum Gravity **39**(22), 225015 (2022). https://doi.org/10.1088/1361-6382/ac9949
26. W. Beordo, M. Crosta, M.G. Lattanzi, P. Re Fiorentin, A. Spagna, Mon. Not. R. Astron. Soc. **529**(4), 4681 (2024). https://doi.org/10.1093/mnras/stae855
27. F. Re, M. Galoppo, (2024). https://doi.org/10.48550/arXiv.2403.03227. arXiv:2403.03227
28. M.L. Ruggiero, J. Cosmol. Astropart. Phys. JCAP **02**(02), 25 (2024)
29. M. Galoppo, D.L. Wiltshire, (2024). https://doi.org/10.48550/arXiv.2406.14157. arXiv:2406.14157
30. M. Galoppo, D.L. Wiltshire, F. Re, (2024). https://doi.org/10.48550/arXiv.2408.00358. arXiv:2408.00358
31. L.F.O. Costa, J. Natário, F. Frutos-Alfaro, M. Soffel, Phys. Rev. D **108**, 044056 (2023)
32. G. Neugebauer, R. Meinel, Phys. Rev. Lett. **75**, 3046 (1995). https://doi.org/10.1103/PhysRevLett.75.3046
33. L. Costa, J. Natário, Phys. Rev. D **110**, 064056 (2024). https://doi.org/10.1103/PhysRevD.110.064056
34. C.J.S. Clarke, *The Analysis of Space-Time Singularities* (Cambridge University Press, Cambridge, 1994)
35. G. Ellis, B.G. Schmidt, Gen. Relativ. Gravit. **8**, 915 (1977)
36. W.J. van Stockum, Proc. R. Soc. Edinb. **57**, 135–154 (1937)
37. W.B. Bonnor, J. Phys. A Math. Gen. **10**, 1673 (1977)
38. W.B. Bonnor, Gen. Relativ. Gravit. **40**, 191–198 (2008)
39. J. Binney, S. Tremaine, *Galactic Dynamics*, 2nd edn. (Princeton University Press, Princeton, 2008). https://doi.org/10.2307/j.ctvc778ff
40. J.A.G. Vickers, Class. Quantum Gravity **4**, 1 (1987)
41. V.B. Bezerra, E.P.S. Shellard, *Cosmic strings and Other Topological Defects* (Cambridge University Press, Cambridge, 1994)
42. M.R. Anderson, *The Mathematical Theory of Cosmic Strings* (CRC Press, Boca Raton, 2002)
43. G. Oliviera-Neto, J. Math. Phys. **37**, 4716–4723 (1996)
44. H. Stephani, D. Kramer, M. MacCallum, C. Hoenselaers, E. Herlt, *Exact Solutions of Einstein's Field Equations* (Cambridge University Press, Cambridge, 2003)
45. R. Geroch, J. Math. Phys. **12**, 918–924 (1971)
46. R. Geroch, J. Math. Phys. **13**, 394–404 (1972)
47. J. Winicour, J. Math. Phys. **16**(9), 1806 (1975)
48. J.N. Islam, *Rotating Fields in General Relativity* (Cambridge University Press, Cambridge, 2009)
49. C.W. Misner, K.S. Thorne, J.A. Wheeler, *Gravitation* (W.H. Freeman and Co Ltd, New York, 1973)
50. E. Poisson, C.M. Will, *Gravity, Newtonian, Post-Newtonian, Relativistic* (Cambridge University Press, Cambridge, 2014). https://doi.org/10.1017/CBO9781139507486
51. F. Bowman, *Introduction to Bessel Functions* (Dover Publications, New York, 2010)
52. Y. Sofue, Publ. Astron. Soc. Jpn. (2013). https://doi.org/10.1093/pasj/65.6.118
53. Y. Sofue, Pub. Astron. Soc. Jpn. **67**(4), 75 (2015). https://doi.org/10.1093/pasj/psv042
54. Z. Xu et al., J. Cosmol. Astropart. Phys. JCAP **2018**(09), 038–038 (2018). https://doi.org/10.1088/1475-7516/2018/09/038
55. K. Jusufi et al., Phys. Rev. D (2019). https://doi.org/10.1103/physrevd.100.044012
56. T. Faber, M. Visser, Mon. Not. R. Astron. Soc. **372**(1), 136 (2006). https://doi.org/10.1111/j.1365-2966.2006.10845.x
57. K.H. Knuth, Dig. Signal Proces. **95**, 102581 (2019). https://doi.org/10.1016/j.dsp.2019.102581
58. J. Goodman, J. Weare, Commun. Appl. Math. Comput. Sci. **5**(1), 65 (2010). https://doi.org/10.2140/camcos.2010.5.65
59. C.F. McKee, A. Parravano, D.J. Hollenbach, Astrophys. J. **814**(1), 13 (2015). https://doi.org/10.1088/0004-637X/814/1/13
60. H. Wang et al., Astrophys. J. **942**(1), 12 (2022). https://doi.org/10.3847/1538-4357/aca27c
61. F.S. Labini, Astrophys. J. **976**(2), 12 (2024)
62. C.R. Keeton, C.S. Kochanek, Astrophys. J. **495**(1), 157 (1998). https://doi.org/10.1086/305272
63. S. Hawking, G. Ellis, *The Large Scale Structure of Space-time* (Cambridge Monograph on Mathematical Physics, Cambridge, 1973)
64. R. Penrose, Phys. Rev. Lett. **14**, 57–59 (1965)
65. S. Hawking, Phys. Rev. Lett. **15**, 689–690 (1965)
66. S. Hawking, R. Penrose, *The Nature of Space and Time* (Princeton University Press, Princeton, 1996)
67. S. Hawking, Phys. Rev. Lett. **17**, 444–445 (1966)
68. S. Hawking, R. Penrose, Proc. R. Soc. Lond. A **314**, 529–548 (1970)
69. F.J. Tipler, Ann. Phys. **108**, 1–36 (1977)
70. C.J. Isham, Proc. R. Soc. Lond. A. **364**, 591–599 (1978)